Atmos. Chem. Phys., 25, 2613–2630, 2025
https://doi.org/10.5194/acp-25-2613-2025

Atmospheric Chemistry and Physics
Open Access
EGU

Research article

Accounting for the black carbon aging process in a two-way coupled meteorology–air quality model

Yuzhi Jin[1,2], Jiandong Wang[1,2], Chao Liu[1,2], David C. Wong[3,4], Golam Sarwar[3], Kathleen M. Fahey[3], Shang Wu[1,2], Jiaping Wang[5,6], Jing Cai[1,2,7], Zeyuan Tian[1,2], Zhouyang Zhang[1,2], Jia Xing[8], Aijun Ding[5,6], and Shuxiao Wang[9,10]

[1]State Key Laboratory of Climate System Prediction and Risk Management, Nanjing University of Information Science and Technology, Nanjing, 210044, China
[2]Collaborative Innovation Center on Forecast and Evaluation of Meteorological Disasters, School of Atmospheric Physics, Nanjing University of Information Science and Technology, Nanjing, 210044, China
[3]Atmospheric and Environmental Systems Modeling Division, US Environmental Protection Agency, Research Triangle Park, NC 27711, USA
[4]Department of Earth and Atmospheric Sciences, University of Houston, Houston, TX 77204, USA
[5]Joint International Research Laboratory of Atmospheric and Earth System Sciences, School of Atmospheric Sciences, Nanjing University, Nanjing, 210023, China
[6]National Observation and Research Station for Atmospheric Processes and Environmental Change in Yangtze River Delta, Nanjing University, Nanjing, 210023, China
[7]Institute for Atmospheric and Earth System Research, Faculty of Science, University of Helsinki, Helsinki, 00014, Finland
[8]Department of Civil and Environmental Engineering, University of Tennessee, Knoxville, TN 37996, USA
[9]State Key Laboratory of Regional Environment and Sustainability, Beijing, 100084, China
[10]School of Environment, Tsinghua University, Beijing, 100084, China

Correspondence: Jiandong Wang (jiandong.wang@nuist.edu.cn) and David C. Wong (wong.david-c@epa.gov)

Received: 26 July 2024 – Discussion started: 8 August 2024
Revised: 20 November 2024 – Accepted: 11 December 2024 – Published: 28 February 2025

Abstract. Black carbon (BC) exerts significant impacts on both climate and environment. The BC aging process alters its hygroscopicity and light absorption properties. Current models, like the Weather Research and Forecasting – Community Multiscale Air Quality (WRF-CMAQ) two-way coupled model, inadequately characterize these alterations. In this study, we accounted for the BC aging process in the WRF-CMAQ model (WRF-CMAQ-BCG). We introduced two new species (bare BC and coated BC) into the model and implemented a module to simulate the conversion from bare BC to coated BC, thereby characterizing the aging process. Furthermore, we improved the wet-deposition and aerosol optical modules to analyze the effects of BC aging on hydrophobicity and light absorption. The simulated results indicate a spatial distribution pattern with bare BC prevalent near emission sources and coated BC more common farther from sources. The average number fraction of coated BC (NF_{coated}) is approximately 57 %. Temporal variation exhibits a distinct diurnal pattern, with NF_{coated} increasing during the daytime. The spatial distribution of wet deposition varies significantly between bare and coated BC. Bare BC exhibits a point-like deposition pattern, whereas coated BC displays a zonal distribution. Notably, coated BC dominates the BC wet-deposition process. Additionally, incorporating the BC aging process reduces BC wet deposition by 17.7 % and increases BC column concentration by 10.5 %. The simulated mass absorption cross-section (MAC) value improved agreement with observed measurements. Overall, the WRF-CMAQ-BCG model enhances the capability to analyze aging-related variables and the BC mixing state while also improving performance in terms of wet deposition and optical properties.

Published by Copernicus Publications on behalf of the European Geosciences Union.

1 Introduction

Black carbon (BC) refers to the aerosol emitted into the atmosphere from incomplete combustion of carbonaceous fuels. As a predominant light-absorbing aerosol, BC exhibits strong absorption capability within the visible wavelength range, surpassing other light-absorbing aerosols (Bond et al., 2013). This pronounced light-absorbing property has significant impacts on climate and air quality (Tan et al., 2020). It influences direct radiative forcing by absorbing and scattering sunlight. It also produces indirect radiative forcing by influencing cloud formation and altering surface albedo when deposited on ice or snow surfaces (Hansen and Nazarenko, 2004; Jacobson, 2004; Ramanathan and Carmichael, 2008). Additionally, BC aerosol can exacerbate regional air pollution by changing local meteorological conditions. The light-absorbing property of BC leads to atmospheric heating, depressing the development of the planetary boundary layer (PBL) and promoting the formation of regional atmospheric pollution (Ding et al., 2016). Moreover, the unique morphology of BC aerosol, which provides a large surface area, facilitates heterogeneous reactions with trace gases, thereby promoting the formation of secondary particulate matter (Zhang et al., 2020). Therefore, BC aerosol is of great significance in both meteorological and environmental fields.

The BC component exhibits very low chemical reactivity and is refractory (Bond et al., 2013). Consequently, previous studies have typically considered BC aerosol to be chemically inert, primarily serving as a reaction interface for other chemical reactions due to its unique morphology (Monge et al., 2010). However, freshly emitted BC aerosol experiences condensation, coagulation, and heterogeneous oxidation processes during atmospheric transport, becoming coated by scattering aerosol components and being converted into aged BC aerosol (some absorbing organics that coat BC are not considered in this study). (Riemer et al., 2009; Oshima and Koike, 2013; Tan et al., 2020). During this transformation, a significant part of BC aerosol changes from an external to an internal mixing state (Pratt et al., 2011; Stevens and Dastoor, 2019). The BC aging process alters the hydrophobicity and light-absorbing property of BC aerosol, thereby affecting cloud condensation nuclei (CCN) concentration, wet deposition, and aerosol optical properties (Yu, 2000; Oshima and Koike, 2013; Bond and Bergstrom, 2006). Therefore, when evaluating the impact of BC aerosol in meteorology and environmental fields, the BC aging process cannot be neglected.

Numerical simulations of BC aerosol have gradually incorporated the effects of the BC aging process. Various aerosol modeling approaches, each with distinct characteristics, have evolved along different developmental trajectories. These models are mainly divided into four categories: bulk model, modal model, sectional model, and particle-resolved model. The bulk model primarily categorizes BC aerosol into hydrophobic and hydrophilic types, conceptualizing the aging process as a conversion from hydrophobic to hydrophilic BC. The global 3-D chemical transport model (GEOS-Chem) is a good representative of the bulk model approach. The default GEOS-Chem model uses a fixed *e*-folding lifetime for this conversion (Park et al., 2003). Huang et al. (2013) added a condensation–coagulation scheme, which is affected by water vapor, ozone, the hydroxyl radical, and sulfuric acid concentration, to the GEOS-Chem model. He et al. (2016) developed a "hybrid" microphysics-based aging scheme for condensation, coagulation, and heterogeneous chemical oxidation processes in the GEOS-Chem model. While the details are continuously refined, these schemes fundamentally represent the BC aging process as a conversion from hydrophobic to hydrophilic BC. The modal model mainly addresses the aging process by representing its different aging states of BC within different modes. An example of this paradigm is the Community Atmosphere Model version 5–Modal Aerosol Module (CAM5-MAM). The three-mode version (MAM3) places BC aerosol in the accumulation mode, assuming it is fully internally mixed. To account for the BC aging process, both the four-mode version (MAM4) (Liu et al., 2016) and the seven-mode version (MAM7) (Liu et al., 2012) use BC in the primary carbon mode to represent freshly emitted BC, which converts to aged BC in the accumulation mode after the aging process. The sectional model expands traditional size bins to two-dimensional size BC proportion bins for considering the BC mixing state during the aging process. For instance, the default Weather Research and Forecasting model coupled with Chemistry (WRF-Chem) includes BC aerosol concentration, without the BC mixing state. Matsui et al. (2013) developed a model resolved by size and BC mixing state based on the WRF-Chem model (MS-resolved WRF-Chem model) that divides BC within each size bin based on mass fraction to describe changes in BC mixing state during the aging process. A representative example of the particle-resolved model is the Particle-resolved Monte Carlo code for atmospheric aerosol simulation (PartMC). When coupled with the Model for Simulating Aerosol Interactions and Chemistry (PartMC–MOSAIC), it can precisely characterize the chemical composition of each particle, thus accurately tracking the aging process of BC aerosol. These four models have integrated respective techniques to deal with the BC aging process, and each model execution time has increased accordingly. Each technique has its own benefits and drawbacks as well as additional computational burden. Therefore, selecting appropriate methods to account for the BC aging process and striking a balance between accuracy and computational burden remain topics of ongoing exploration.

The Community Multiscale Air Quality (CMAQ) model, developed by the US Environmental Protection Agency (EPA), is widely used in the research community as well as

by the US government as a regulatory model, and it continues to evolve. To account for the interactive two-way feedback between aerosols and meteorological conditions, Wong et al. (2012) developed the Weather Research and Forecasting – Community Multiscale Air Quality (WRF-CMAQ) two-way coupled model. The mixing state of BC aerosol is simplified to a fully internally mixed state in the CMAQ model. When considering the influence of aerosols on meteorology, this simplification has a more pronounced impact. Therefore, incorporating the BC aging process in the WRF-CMAQ model is essential, as it significantly influences hydrophobicity and light absorption. In this study, we accounted for the BC aging process in the WRF-CMAQ model (WRF-CMAQ-BCG) by introducing two new species and constructing a BC aging module. Furthermore, we improved the wet-deposition module and aerosol optical module to investigate the effects of changes in hydrophobicity and light absorption caused by the BC aging process. Section 2 describes the overall construction of the WRF-CMAQ-BCG model and the development methods for each module. Section 3 provides the case description used for simulation and the model evaluation. The performance of the new model regarding aging-related variables, the BC mixing state, BC wet deposition, and aerosol optics is presented in Sect. 4.

2 The WRF-CMAQ-BCG model

2.1 New model

During the aging process, BC aerosol becomes coated with other aerosol components, changing from an externally mixed state to an internally mixed state. This process converts hydrophobic BC into hydrophilic BC, enabling it to act as cloud condensation nuclei (CCN), thereby influencing the aerosol indirect radiative effect. Concurrently, the coating acquired during aging enhances BC's absorption properties through the lensing effect (Lack and Cappa, 2010). This amplification of absorption directly impacts overall radiation dynamics, underscoring the profound influence of BC aging on both direct and indirect aerosol–radiation interactions in the atmosphere (the EPA's publicly released WRF-CMAQ model does not yet have an indirect radiative effect capability). The original WRF-CMAQ model does not account for the BC aging process (Fig. 1, left panel). The model assumes that freshly emitted BC aerosol undergoes instantaneous aging, resulting in a uniformly fully internally mixed state without spatiotemporal variation. To address this limitation, we developed the WRF-CMAQ-BCG model, capable of handling the main changes in BC aerosol properties due to aging throughout the entire atmospheric life cycle, from emission to deposition (Fig. 1, right panel).

To differentiate the aging states of BC aerosol, we introduced two new species: "bare BC (ABEC)" and "coated BC (ACEC)" in our model (Table 1). They replace the single "BC (AEC)" in the original model. Bare BC represents unaged, hydrophobic, externally mixed BC aerosol, while coated BC represents aged, hydrophilic, internally mixed BC aerosol. It is important to note that bare BC and coated BC are used to differentiate the aging states of BC aerosol, and their combination is equivalent to the BC in the original WRF-CMAQ model.

Table 1. New species added in the model.

	Aging state	Mixing state	Hygroscopicity
Bare BC	Unaged	External	Hydrophobic
Coated BC	Aged	Internal	Hydrophilic

The WRF-CMAQ model provides meteorological and chemical conditions for the BC aging process, while the BC aging process in turn, influences the meteorology and air quality simulated by the model. This continuous and cyclic interaction in the WRF-CMAQ coupled model provides a realistic representation of the atmospheric processes. The primary differences between bare BC and coated BC lie in their hydrophobicity and light absorption property. Changes in hydrophobicity mainly affect aqueous chemistry, scavenging, and wet deposition, while changes in the light absorption property affect aerosol optical calculations. For other atmospheric processes, including advection, diffusion, turbulence, and dry deposition, the behavioral differences between bare BC and coated BC are minimal. Consequently, the emission module, wet-deposition module, and aerosol optical module of the WRF-CMAQ-BCG model require relevant updates based on the inclusion of the BC aging process, as shown in Table 2. In the original model, BC aerosol did not include the aging process and was treated as being in a completely internally mixed state. This approach neglected the presence and impact of externally mixed BC aerosol in the real atmosphere, leading to inaccuracy in the numerical simulation of BC aerosol. In our new model, the differences in BC aerosol across major processes under different aging states are considered. Freshly emitted BC aerosol (bare BC) enters the BC aging module from the emission module and is gradually converted into coated BC through the aging process. When bare BC and coated BC enter the wet-deposition module, hydrophobic bare BC cannot undergo nucleation scavenging during in-cloud scavenging, in turn affecting the wet deposition of BC aerosol. Bare BC exists in an external mixing state, whereas coated BC has stronger light absorption due to the lensing effect. Therefore, bare BC and coated BC need to be considered separately when calculating aerosol optics.

2.2 BC aging module

In the WRF-CMAQ-BCG model, we constructed a specialized BC aging module to account for the BC aging process in the atmosphere. The aging process is represented by the conversion from bare BC to coated BC. The development

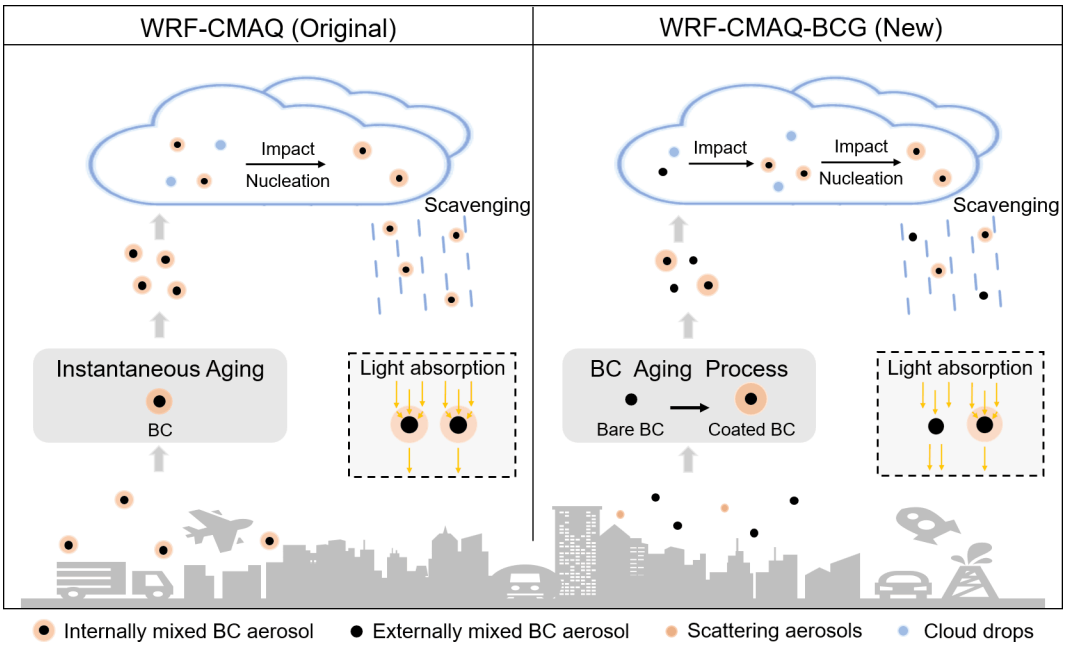

Figure 1. The BC mixing state in the WRF-CMAQ model and the WRF-CMAQ-BCG model.

Table 2. Comparison of BC aerosol in major processes (Aitken and accumulation modes).

Processes		BC (original)	Bare BC (new)	Coated BC (new)
Emission		Yes	Yes	No
BC aging		No aging process	Bare BC is aged to become coated BC	
Wet deposition	Impact scavenging	Yes	Yes	Yes
	Nucleation scavenging	Yes	No	Yes
Aerosol optics		Core–shell sphere	Homogeneous sphere	Core–shell sphere

of appropriate aging schemes is crucial for accurately simulating this dynamic conversion process. The aging rate and the aging timescale are two important variables related to the aging process. The aging rate indicates the speed of the aging process as shown in Eq. (1), while the aging timescale reflects the time required for the aging process, inversely related to the aging rate, as shown in Eq. (2). Global climate and atmospheric chemical transport models often employ a simplified approach to carbonaceous aerosol aging, typically using a uniform aging timescale of approximately 1 d (Huang et al., 2013). For two specific examples, the traditional GEOS-Chem model (Park et al., 2003) and the Regional Climate Model (RegCM) (Solmon et al., 2006) both set a fixed conversion lifetime of 1.15 d. This constant aging scheme is computationally efficient but cannot capture the dynamic changes in the aging process. Consequently, some researchers have developed more sophisticated approaches, parameterizing the aging rate and linking it to specific atmospheric components (Huang et al., 2013; Croft et al., 2005). The hydroxyl (OH) radical, a key player in atmospheric chemistry, facilitates the conversion of sulfur dioxide (SO_2) to sulfuric acid (H_2SO_4). The condensation of H_2SO_4 gas onto the surface of particles leads to the conversion of carbonaceous aerosols from hydrophobic to hydrophilic. Recognizing this relationship, some studies have used the OH radical to parameterize the aging rate of BC (Liu et al., 2011; Huang et al., 2013; Oshima and Koike, 2013).

The aging rate (k) and the aging timescale (τ) are shown in Eqs. (1) and (2):

$$k = \frac{\partial(M_{\text{coated}})/\partial t}{M_{\text{bare}}}, \quad (1)$$

$$\tau = \frac{1}{k}, \quad (2)$$

where M_{bare} and M_{coated} are the mass concentration of bare BC and coated BC aerosol, respectively.

This study employs a BC aging module that quantifies the BC aging rate using an equation dependent on the concentration of OH radicals, as shown in Eq. (3). Condensation is considered through the setting of a fast-aging term, while co-

agulation is considered through a slow-aging term. Although coagulation can occur rapidly near sources, it does not play a dominant role within the context of mesoscale modeling compared to condensation (Doran et al., 2008; Oshima et al., 2009; Riemer et al., 2010; Zaveri et al., 2010). Based on the selected OH aging scheme, the dynamic process of BC aging is represented by setting a virtual reaction, wherein bare BC is progressively converted into coated BC. The aging rate is used as the reaction rate for this virtual chemical reaction.

$$k = \beta\,[\mathrm{OH}] + \alpha, \tag{3}$$

where k represents the aging rate and [OH] represents the OH radical concentration. β and α are assumed to be constant, with values of 4.6×10^{-12} cm^3 molec.$^{-1}$ s^{-1} and 5.8×10^{-7} s^{-1}, respectively; β is estimated by assuming an e-folding aging timescale of 2.5 d for condensation; and α is estimated by assuming a 20 d e-folding lifetime for coagulation (Liu et al., 2011; Huang et al., 2013; Oshima and Koike, 2013). However, this constant assumption does not account for the dynamic variations in the coagulation and condensation processes, which could introduce some bias.

2.3 Wet-deposition module

The removal pathways for BC aerosol in the atmosphere are dry and wet deposition (Begam et al., 2016; Bibi et al., 2017), with wet deposition accounting for nearly 80 % (Textor et al., 2006; Choi et al., 2020). While dry deposition is primarily governed by surface characteristics and meteorological conditions, showing minimal sensitivity to BC aging, this study prioritizes wet-deposition processes.

In the WRF-CMAQ model, the wet-deposition module carries out the following tasks: calculation of in-cloud scavenging and precipitation scavenging of BC aerosol, performance of aqueous chemistry calculations, and accumulation of wet deposition. Precipitation scavenging is associated with precipitation forms such as rain, snow, and graupel and is minimally affected by changes in BC aerosol properties before and after aging. Therefore, this study does not consider the differences in the precipitation scavenging process. In contrast, in-cloud scavenging (which includes nucleation scavenging and impact scavenging) is strongly associated with the BC aging process, reflecting the hydrophobicity differences between bare BC and coated BC. Nucleation scavenging refers to the process where aerosols serve as CCN, becoming cloud droplets enveloped by cloud water and being subsequently removed. Impact scavenging occurs through collisions with cloud droplets (Barrett et al., 2019). In the WRF-CMAQ model, removal rates are computed using cloud water content and the precipitation rate. The original model further differentiates scavenging mechanisms based on particle size: BC aerosol in the accumulation mode undergoes nucleation scavenging, while BC aerosol in the Aitken mode experiences impact scavenging as interstitial aerosol (Binkowski and Roselle, 2003). The hydrophobicity changes caused by the BC aging process mainly affect nucleation scavenging because hydrophobic bare BC cannot act as CCN, while hydrophilic coated BC can. In other words, bare BC cannot undergo nucleation scavenging. Within the framework of the WRF-CMAQ model, we modified the wet-deposition algorithm to ensure that hydrophobic bare BC in the accumulation mode is not removed by nucleation scavenging, while Aitken-mode bare BC undergoes impact scavenging. After impact scavenging, bare BC is converted into coated BC due to water envelopment, which continues its removal from the atmosphere, as illustrated in the right panel of Fig. 1. Overall, these updates to the wet-deposition module, described in this work, enhance the representation of BC aerosol in various aspects.

2.4 Aerosol optics module

BC aerosol, a dominant light-absorbing atmospheric constituent, plays a crucial role in estimating direct radiative forcing. As BC ages, the BC component becomes coated by other components, which act like lenses, refracting more light onto the BC aerosol and significantly enhancing its light absorption (Lack and Cappa, 2010). The WRF-CMAQ model assumes a fully internally mixed state for BC, treating all BC aerosol as coated. This approach neglects the presence of externally mixed bare BC in the atmosphere, leading to an overestimation of the overall light absorption by aerosols. The third part of this work will address this limitation.

In the WRF-CMAQ model, the light absorption of aerosols is entirely attributed to BC aerosol. BC aerosol is considered the core, with water-soluble aerosols, insoluble aerosols, aerosol water, and sea salt as the shell. Each substance has its corresponding refractive index across 14 wavelengths under the Rapid Radiative Transfer Model (RRTM) for global climate model (GCM) applications (RRTMG) scheme. For aerosols containing BC in the Aitken and accumulation modes, core–shell Mie theory is employed to calculate their optical characteristics (coarse-mode aerosols without a BC component are not considered in this study). The particle structure information cannot be fully represented in the current WRF-CMAQ model, as the spherical shape assumption is used for calculations. This simplification may introduce biases into the results (He et al., 2015; Wang et al., 2017, 2021). The potential impacts of such structural simplifications are not addressed in this study. In our WRF-CMAQ-BCG model, we calculated the optics of bare BC and coated BC separately in the Aitken and accumulation modes, without accounting for the presence of scattering aerosols independently. This omission may result in an overestimation of the coating thickness, potentially introducing some bias into the optical simulation results (Chen et al., 2023). We introduced a variable, the number fraction of coated BC ($\mathrm{NF_{coated}}$). The $\mathrm{NF_{coated}}$ variable was brought into the aerosol optical module for translating the BC core back to bare BC and coated BC. Only coated BC can be a core surrounded by a shell. Once

encapsulated, coated BC becomes a BC-containing particle, represented as a core–shell sphere, and its particle size information is recalculated based on the volume of the coated BC core and the shell. Its optical properties are calculated using core–shell Mie theory. In contrast, bare BC is represented as a homogeneous sphere, with the particle size recalculated using the volume of bare BC, and its optical properties are calculated using standard Mie theory. By apportioning the BC core, the overestimation of aerosol light absorption can be corrected.

$$\mathrm{NF}_{\mathrm{coated}} = \frac{N_{\mathrm{coated}}}{N_{\mathrm{bare}} + N_{\mathrm{coated}}} = \frac{V_{\mathrm{coated}}}{V_{\mathrm{bare}} + V_{\mathrm{coated}}} = \frac{M_{\mathrm{coated}}}{M_{\mathrm{bare}} + M_{\mathrm{coated}}}, \quad (4)$$

where $\mathrm{NF}_{\mathrm{coated}}$ represents the number fraction of coated BC and N_{bare} and N_{coated} are the number concentration of bare BC and coated BC aerosol, respectively. V_{bare} and V_{coated} are the volume of bare BC and coated BC aerosol, respectively. M_{bare} and M_{coated} are the mass concentration of bare BC and coated BC aerosol, respectively. Bare BC and coated BC are merely in different aging states; they are essentially BC aerosol with the same density and volume. Therefore, the number fraction of coated BC can be calculated from the mass fraction of coated BC.

3 Case description and model evaluation

To evaluate the performance of the new model and analyze the BC aging process, we conducted a simulation using the WRF-CMAQ-BCG model with WRF version 4.4.1 and CMAQ version 5.4 over the continental United States (CONUS) domain for the entire month of June 2010. The model uses a horizontal spatial resolution of 12 km with 35 vertical layers. A 1-month spin-up period (May 2010) was utilized to initialize the model. The initial and boundary conditions were configured with equal proportions of bare BC and coated BC. The WRF model parameterization schemes selected for the simulation case are listed in Table 3. The CMAQ model employs the "cb6r5_AERO7" chemical mechanism and utilizes the Rosenbrock solver. Additionally, we applied the four-dimensional data assimilation (FDDA) technique within the WRF model framework to improve the meteorological fields during the simulation. Specifically, we used analysis nudging to assimilate with a 3 h frequency. The assimilated data are sourced from the North American Mesoscale Forecast System (NAM), provided by the National Weather Service's National Centers for Environmental Prediction (NCEP). The nudging variables included horizontal winds (U and V), temperature (T), and the water vapor mixing ratio (Q). In the WRF-CMAQ coupled model scenario, the nudging strength was set to a very low value (Gilliam et al., 2012) to minimize interference with the model dynamics while constraining the meteorological fields.

Figure 2 illustrates the spatial distribution of BC emissions on the simulation domain in red, and the blue star represents the ground observation station T0 of the Carbonaceous Aerosols and Radiative Effects Study (CARES) campaign, located in Sacramento, California. The observation dataset is available from the Atmospheric Radiation Measurement (ARM) program of the US Department of Energy (DOE) (https://adc.arm.gov/discovery/#/results/s::CARES, last access: 4 January 2024). This comprehensive campaign collected a diverse array of data, encompassing aerosols, atmospheric conditions, cloud properties, and radiation data. The accuracy of the dataset has been widely recognized (Zaveri et al., 2012; Cahill et al., 2012). Data collected from this site are used as the benchmark for site evaluation and comparison, and the data used in our study are presented in Table 4. The data sources for the regional-scale model evaluation and analysis of results are provided in the Supplement.

To evaluate the accuracy of meteorological and chemical conditions for considering the BC aging process in this study, we compared the simulation results of the WRF-CMAQ model and the WRF-CMAQ-BCG model with various meteorological observations, as well as with the volumetric concentrations of several gases at the T0 site in the CARES campaign. Figure 3 illustrates the comparison of meteorological data, including temperature (T), relative humidity (RH), atmospheric pressure (P), wind speed (WS), and wind direction (WD). The resulting mean bias errors (MBEs) for these variables were 0.14 K, 1.14 %, 0.79 hPa, 0.50 m s^{-1}, and 28.92°, respectively, in the WRF-CMAQ model and 0.13 K, 1.19 %, 0.79 hPa, 0.50 m s^{-1}, and 28.33°, respectively, in the WRF-CMAQ-BCG model. Figure 4 presents the model and observation comparison of four gases – O_3, SO_2, NO, and NO_2 – at the T0 site, based on the MBE metric. The resulting values for these gases compared to the observations were −7.83, 0.077, 1.42, and 2.91 ppbv, respectively, in the WRF-CMAQ model and −7.87, 0.074, 1.43, and 2.91 ppbv, respectively, in the WRF-CMAQ-BCG model. These results demonstrate that both the WRF-CMAQ model and the WRF-CMAQ-BCG model exhibit good accuracy and have insignificant differences. Clearly, the inclusion of the BC aging process does not degrade the original model's accuracy in simulating these common variables, and the models can provide reasonably accurate meteorological and chemical conditions for the aging process.

4 Results

4.1 Aging-related variables

The aging rate (k) and the aging timescale (τ) are important variables to quantify the aging process. The standard WRF-CMAQ model lacks the capability to generate BC aging-related variables. In contrast, in the WRF-CMAQ-BCG model, spatiotemporal variations in the aging-associated variables in the BC aging process are related to the

Table 3. Setup of physical process schemes in WRF model simulation.

Physical processes	Schemes	References
Microphysics	Morrison two-moment scheme	Morrison et al. (2009)
Planetary boundary layer physics	Asymmetric Convection Model version 2 scheme	Pleim (2007)
Cumulus parameterization	Kain–Fritsch cumulus potential Scheme	Kain (2004)
Shortwave and longwave	RRTMG shortwave and longwave schemes	Iacono et al. (2008)
Land surface	Pleim–Xiu land surface model	Pleim and Gilliam (2009)
Surface layer	Pleim–Xiu scheme	Pleim (2006)

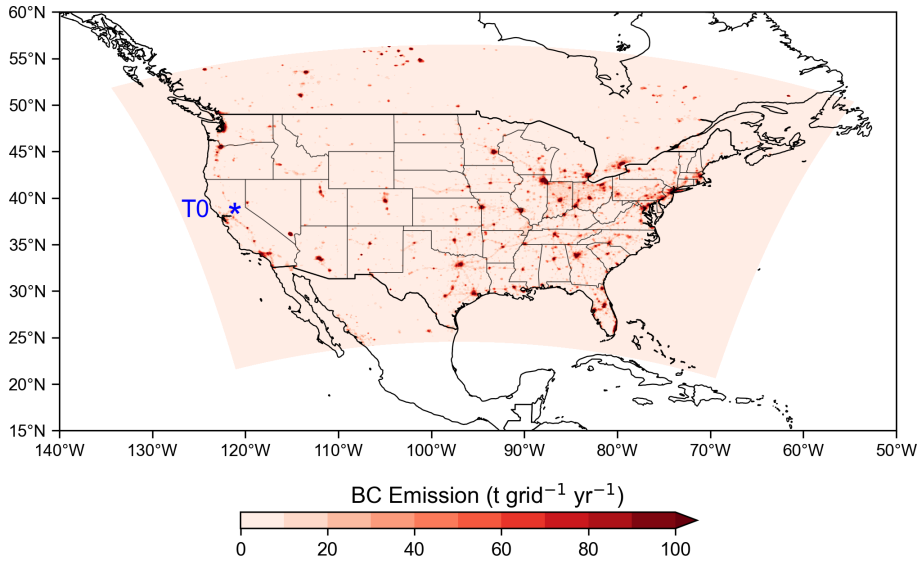

Figure 2. Spatial distribution of BC emissions for June 2010 over the model simulation area (red color). The blue star indicates an observation site, T0 (38.6483° N, 121.3493° W).

concentration of OH radicals. The areas with higher values reflect higher atmospheric oxidizing capacity and more active photochemical reactions, leading to a higher aging rate. Figure 5a shows the aging rate, with higher values in the central region corresponding to the dark-orange areas and lower values in the southeastern and western parts corresponding to the yellow areas. The average value is $2.26 \times 10^{-5}\ s^{-1}$. The spatial distribution of the aging timescale shown in Fig. 5b exhibits a reciprocal pattern, with an average aging timescale of 17.49 h, which is close to the value of 18 h obtained by Peng et al. (2016) in Houston.

4.2 Mixing state

The mixing state is a key microphysical characteristic of BC aerosol and a major feature that undergoes significant changes in the aging process. As aging progresses, BC transforms from a completely externally mixed state to a more complex configuration where internally mixed BC and externally mixed BC coexist. Therefore, we can use the number fraction of coated BC (NF_{coated}) to represent the mixing state of BC aerosol.

Regarding the spatial distribution of BC aerosol, as illustrated in Fig. 6, the simulated results of the WRF-CMAQ-BCG model demonstrate that high mass concentrations of bare BC and coated BC are primarily distributed in the eastern United States and the West Coast region. This can be attributed to the higher population density and the presence of heavy industrial and commercial activities in those regions, resulting in a notable increase in BC emissions (as shown in Fig. 2). The simulated mean mass concentration of bare BC (M_{bare}) in the US region is $0.045\ \mu g\ m^{-3}$, while the mean mass concentration of coated BC (M_{coated}) is $0.034\ \mu g\ m^{-3}$. The simulated mean NF_{coated} in the US region is 57 %. The spatial distribution of the mixing state shows that bare BC predominates in the eastern United States and on the West Coast, while coated BC is more prevalent in most of the western region. This phenomenon arises from the more extensive distribution of BC emissions in the eastern region and on the West Coast, leading to a dominance of bare BC. In contrast, in the western region (excluding the West Coast), where BC emissions are less widespread, aging and transport processes play a more significant role, resulting in a higher proportion of coated BC. In summary, the BC mixing state exhibits a

Table 4. Description of T0 site observation data.

Data type	Data	Data description	Instrument/technique
Meteorology	T	Temperature	Vaisala WXT510
	RH	Relative humidity	Vaisala WXT511
	P	Pressure	Vaisala WXT512
	WS	Wind speed	Vaisala WXT513
	WD	Wind direction	Vaisala WXT514
Gas	O_3	O_3 concentration	UV absorption
	SO_2	SO_2 concentration	Thermo Fisher Scientific model 43i
	NO	NO concentration	Chemiluminescence
	NO_2	NO_2 concentration	Photolytic conversion CU GMAX-DOAS
BC	M_{BC}	BC mass concentration	Single-particle soot photometer (SP2)
Optical properties	b_{abs}	Absorption coefficient	Photoacoustic spectroscopy (PAS)

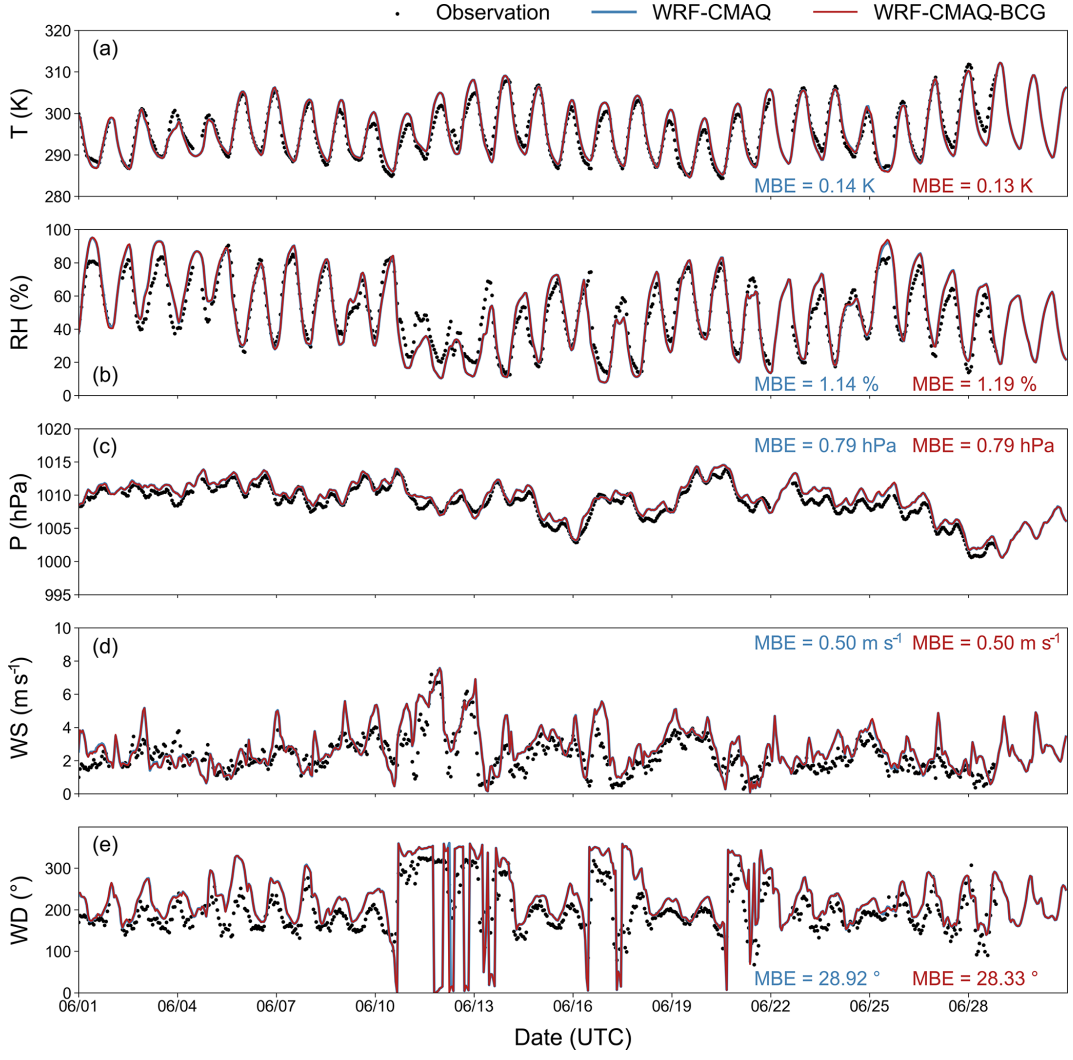

Figure 3. Comparison of simulated and observed meteorological data: **(a)** temperature (T), **(b)** relative humidity (RH), **(c)** pressure (P), **(d)** wind speed (WS), and **(e)** wind direction (WD).

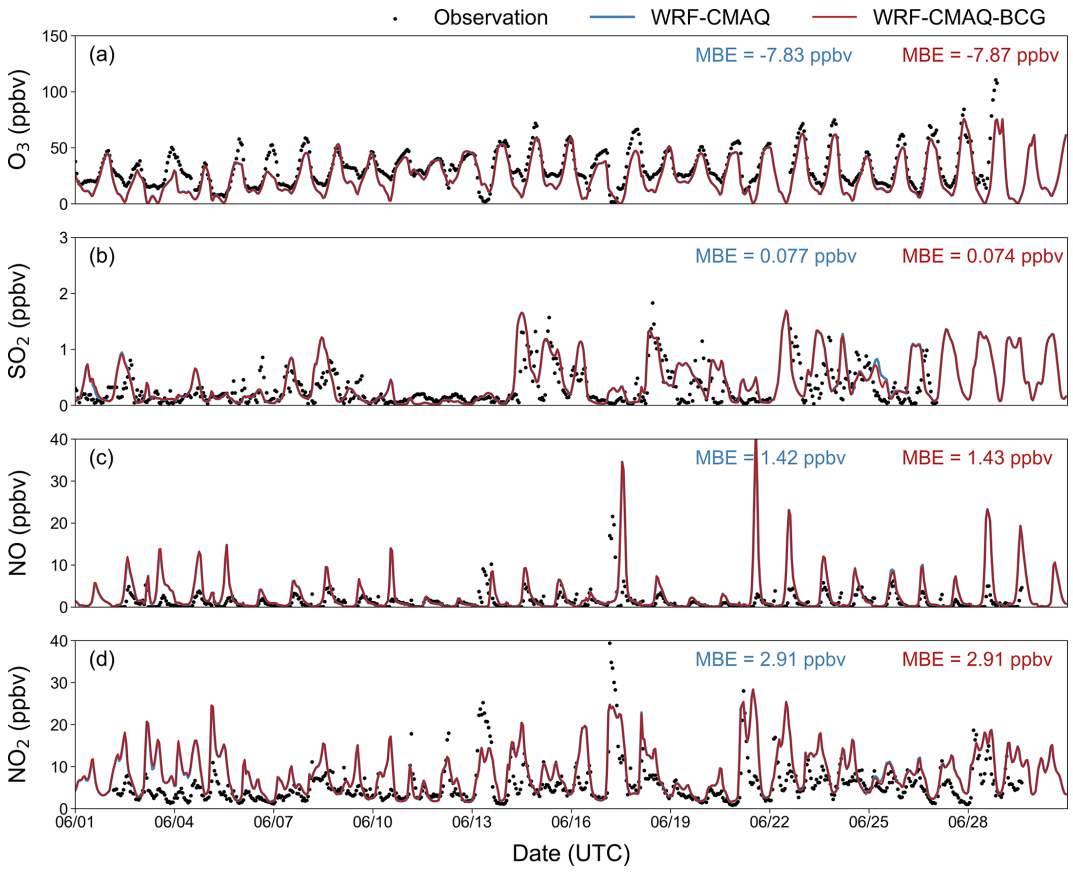

Figure 4. Comparison of simulated and observed concentrations of several gases: **(a)** O_3 concentration, **(b)** SO_2 concentration, **(c)** NO concentration, and **(d)** NO_2 concentration.

distinct pattern: bare BC predominates in proximity to emission sources, while coated BC becomes more prevalent in regions distant from these sources, a result of transport.

We examined the BC mixing state at the T0 site to explore the temporal variations in BC aerosol. Figure 7 presents the daily average variation in BC mixing states at the T0 site. It should be noted that this site is near the emission sources, illustrated by elevated mass concentrations and a higher proportion of bare BC. Figure 7 also shows that the mass concentration of bare BC noticeably decreases in the afternoon, while the mass concentration of coated BC significantly increases during this time. This pattern can be attributed to two primary factors: firstly, the diurnal variation in traffic emissions, which typically peak during morning and evening rush hours, and secondly, the intense solar radiation during the daytime, which enhances photochemical reactions (Peng et al., 2016) and thereby accelerates BC aging and increases coated BC concentrations during the day. As a result, the number fraction of simulated coated BC shows a distinct increase from 08:00 to 20:00 local time, peaking in the afternoon. This finding is similar to the conclusions of Shen et al. (2023). Many observational results also provide evidence for our conclusion, as shown in Fig. 7d (Lan et al., 2013; Huang et al., 2012a, b; Wang et al., 2014a, b, 2016, 2018; Zhang et al., 2018). Due to the variability in BC mass concentrations and mixing states across different regions and times, we normalized NF_{coated} to facilitate quantitative comparison, as shown in Eq. (5). By comparing the simulated and observed normalized NF_{coated}, it is evident that the BC mixing state reflects a temporal-variation characteristic, with the proportion of coated BC significantly increasing during the daytime.

$$\text{Normalized } NF_{coated} = \frac{NF_{coated} - NF_{coated\_min}}{NF_{coated\_max} - NF_{coated\_min}}, \quad (5)$$

where NF_{coated}_min is the minimum value of NF_{coated} and NF_{coated}_max is the maximum value of NF_{coated}.

4.3 Wet deposition

Wet deposition is an important mechanism for the removal of BC aerosol from the atmosphere. The aging process significantly alters the hydrophobic nature of BC aerosol, consequently affecting its susceptibility to in-cloud scavenging.

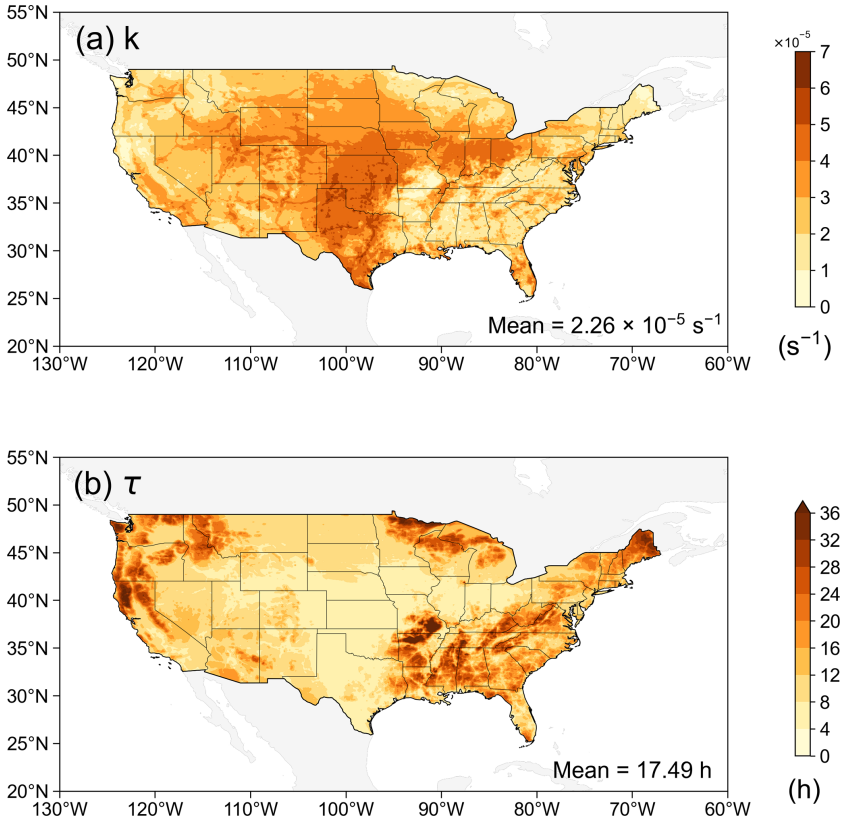

Figure 5. Spatial distribution of aging-related variables (average hourly values for June): **(a)** the aging rate (k) and **(b)** the aging timescale (τ).

The quantity of BC wet deposition serves as a prominent indicator of this effect. The distribution of bare BC wet deposition (W_{bare}) exhibits a characteristic point-like pattern in Fig. 8a. This distinctive distribution is attributed to the spatial distribution of bare BC concentration and the fact that bare BC cannot be removed by nucleation scavenging. In contrast, coated BC undergoes in-cloud scavenging and can be transported more widely by atmospheric processes, so coated BC wet deposition (W_{coated}) exhibits a zonal distribution (see Fig. 8b). These contrasting deposition patterns provide valuable insights into the life cycle and transport mechanisms of BC aerosol in the atmosphere. The point-like distribution of bare BC wet deposition underscores the rapid aging and indicates a localized impact of fresh BC emissions, while the zonal distribution of coated BC wet deposition highlights the role of aging in enhancing BC's atmospheric mobility and its potential for long-range transport. Additionally, the average wet deposition of bare BC is 1.31×10^{-7} mg m^{-2} d^{-1}, whereas the average wet deposition of coated BC is 3.02×10^{-2} mg m^{-2} d^{-1}, differing by 5 orders of magnitude. Therefore, we can conclude that the wet deposition of BC aerosol is primarily due to coated BC.

For the overall wet deposition of BC aerosol, the spatial distribution simulated by the WRF-CMAQ-BCG model is consistent with that simulated by the WRF-CMAQ model, mainly concentrated in the northeastern CONUS domain (Fig. 9). The average BC wet deposition simulated by the WRF-CMAQ-BCG model in the USA is 3.02×10^{-2} mg m^{-2} d^{-1}, which is approximately 17.7 % less than the 3.67×10^{-2} mg m^{-2} d^{-1} simulated by the WRF-CMAQ model. This reduction is because the WRF-CMAQ-BCG model categorized a portion of BC as hydrophobic bare BC, which was not involved in nucleation scavenging, leading to a decrease in BC wet deposition. The 17.7 % reduction highlights the significant impact of the BC mixing state.

The reduction in BC wet deposition may further alter the concentration of BC aerosol in the atmosphere. To investigate this potential scenario, we compared the surface BC mass concentration and column concentration between the two models, WRF-CMAQ and WRF-CMAQ-BCG (Fig. 10). The spatial distribution of BC mass concentration simulated by both models is similar. The average surface BC mass concentration (M_{surBC}) simulated by the original model is 7.48×10^{-2} µg m^{-3}, while in the new model, the average is 7.96×10^{-2} µg m^{-3}, indicating an increase in BC mass concentration. Similarly, the BC column concentration (M_{colBC}) increases from an average of 0.19 mg m^{-2} in the WRF-CMAQ model to 0.21 mg m^{-2} in the WRF-CMAQ-BCG

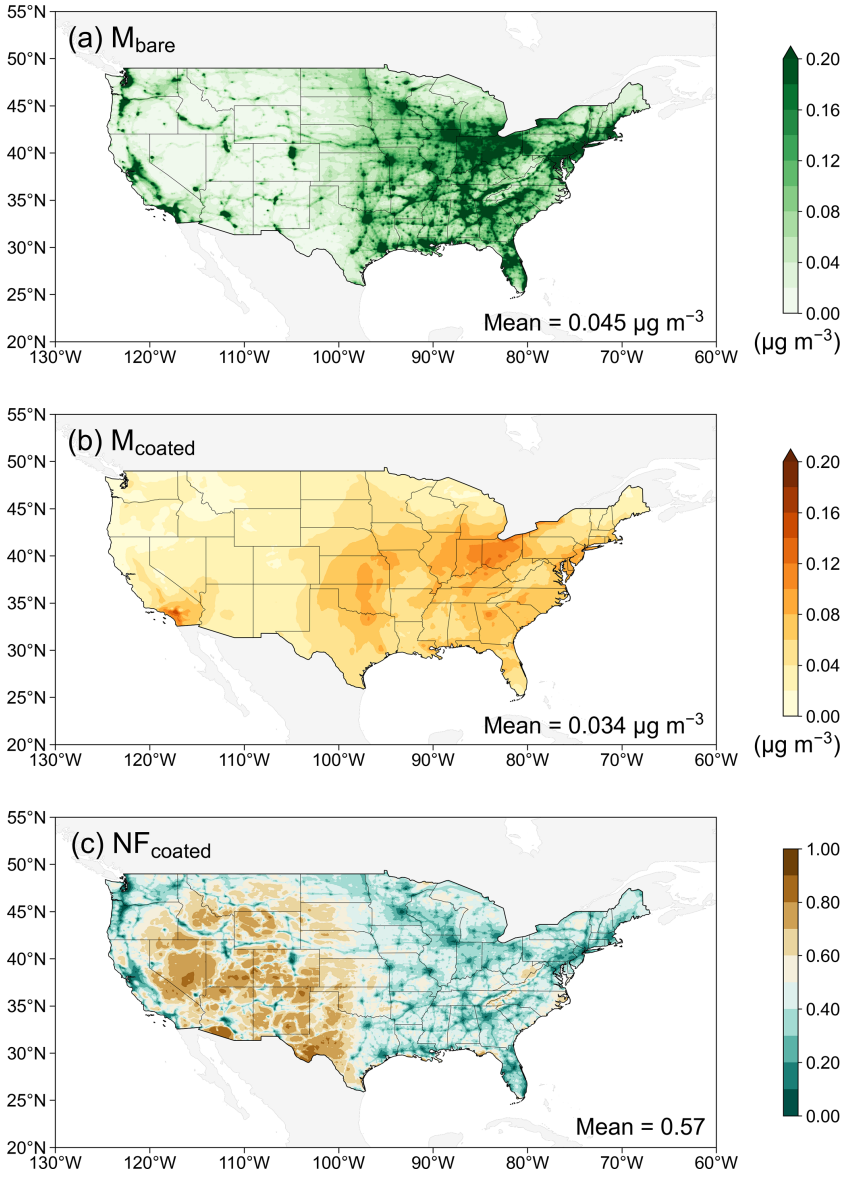

Figure 6. The spatial distribution of **(a)** bare BC mass concentration (M_{bare}), **(b)** coated BC mass concentration (M_{coated}), and **(c)** the number fraction of coated BC (NF_{coated}), with average hourly values for June.

model, with an increase of 10.5 %. This indicates that the fully internally mixed assumption, which does not account for the aging process, overestimates BC wet deposition and thus underestimates BC mass concentration.

4.4 Optical properties

The aging process profoundly influences the optical properties of BC, in particular, the light-absorbing aspect. This study analyzed two key optical parameters at the 532 nm wavelength, the absorption coefficient (b_{abs}) and the BC mass absorption cross-section (MAC), to investigate the changes in BC optical properties before and after accounting for the aging process (Yuan et al., 2021). The MAC values can be calculated as

$$\mathrm{MAC} = \frac{b_{abs}}{M_{BC}}, \tag{6}$$

where M_{BC} represents BC mass concentration.

We compared the time series plots of b_{abs}, M_{BC}, and MAC values simulated by the WRF-CMAQ model and the WRF-CMAQ-BCG model with the observed values at the T0 site (Fig. 11). For b_{abs}, the mean bias error (MBE) value for the WRF-CMAQ model is 0.34×10^{-5} m^{-1}, while for the WRF-CMAQ-BCG model it is 0.19×10^{-5} m^{-1}, representing a 44 % reduction. The simulated M_{BC} values for both models show little difference, with both MBE values being 0.30 μg m^{-3}. For MAC, the MBE value for the WRF-

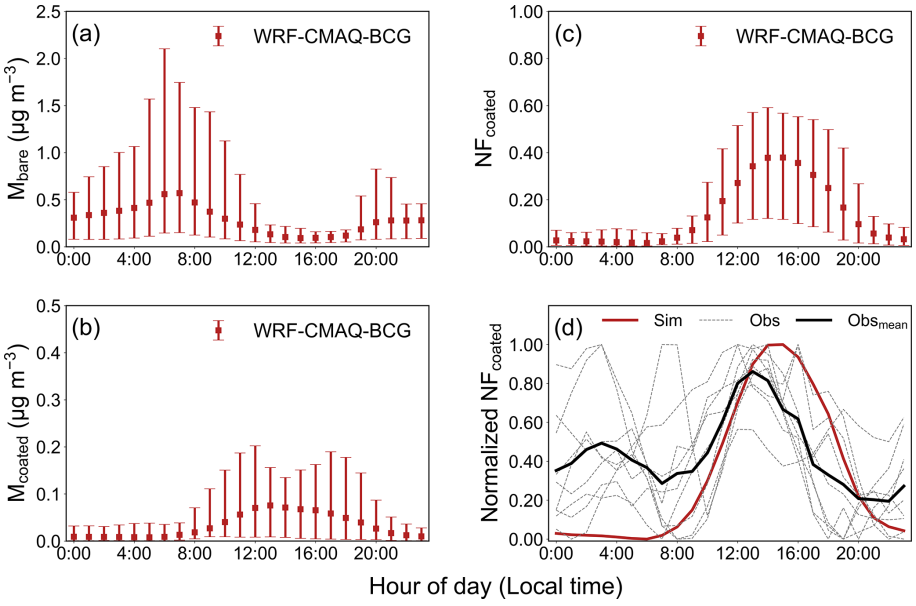

Figure 7. Daily average variation in simulated results: **(a)** bare BC mass concentration (M_{bare}), **(b)** coated BC mass concentration (M_{coated}), **(c)** number fraction of coated BC (NF_{coated}), and **(d)** normalized NF_{coated} compared with other observational studies.

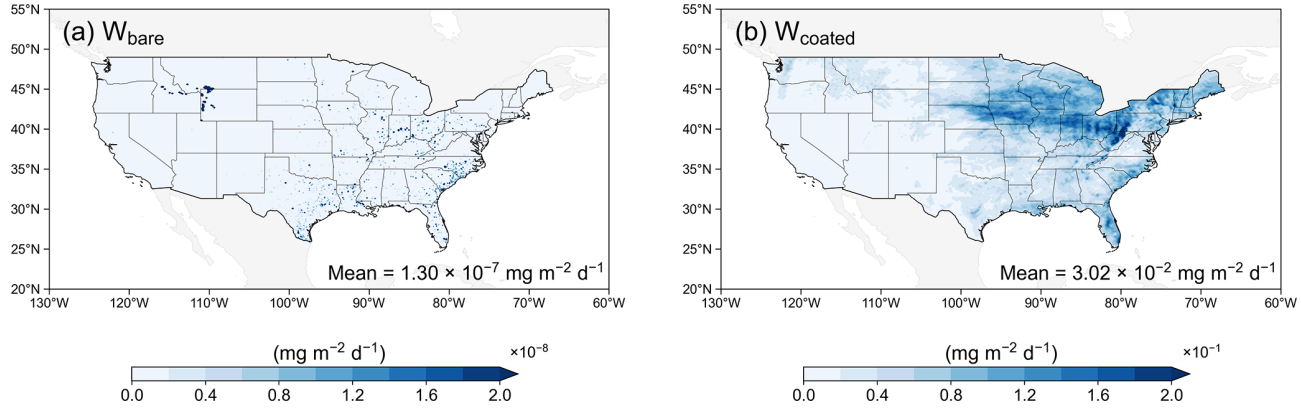

Figure 8. Wet deposition of **(a)** bare BC (W_{bare}) and **(b)** coated BC (W_{coated}) simulated by the WRF-CMAQ-BCG model, with average hourly values for June.

CMAQ model is 2.63 $m^2 g^{-1}$, whereas the WRF-CMAQ-BCG model yields an MBE of $-1.24\ m^2 g^{-1}$, demonstrating a significant reduction. The new model, which incorporated the aging process, demonstrates accuracy improvement in simulating b_{abs} values with respect to observation data. However, the discrepancies in BC mass concentration (M_{BC}) between the two models are minimal, suggesting that variations in M_{BC} play a minor role in the observed changes in the MAC values. This indicates that the main contributing factor to the optical impact of BC aging is the alteration in BC mixing state during the aging process, rather than BC concentration.

We also analyzed the performance of MAC values at the T0 site with statistical data covering hourly observations and simulated results for June. As shown in Fig. 12, the median observed value of MAC is 9.75 $m^{-2} g^{-1}$, while the median value from the original WRF-CMAQ model is 12.45 $m^{-2} g^{-1}$, resulting in a difference of 2.7 $m^{-2} g^{-1}$. In contrast, the median value from the WRF-CMAQ-BCG model is 8.77 $m^{-2} g^{-1}$, which is closer to the observed median value. Furthermore, the broader sections within each type of plot depict the primary distribution of MAC values, which are the most frequently occurring values. It is evident that the WRF-CMAQ-BCG model results are closer to the observations than those of the WRF-CMAQ model. We conclude that the WRF-CMAQ-BCG model simulates the optical properties of BC aerosol in a more precise manner.

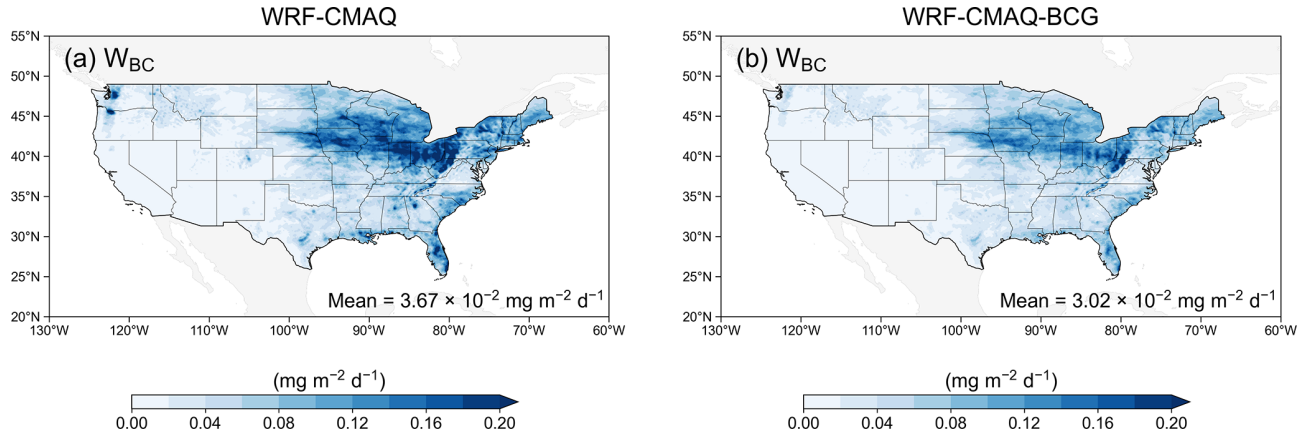

Figure 9. BC wet deposition (W_{BC}) simulated by **(a)** the WRF-CMAQ model and **(b)** the WRF-CMAQ-BCG model, with average hourly values for June.

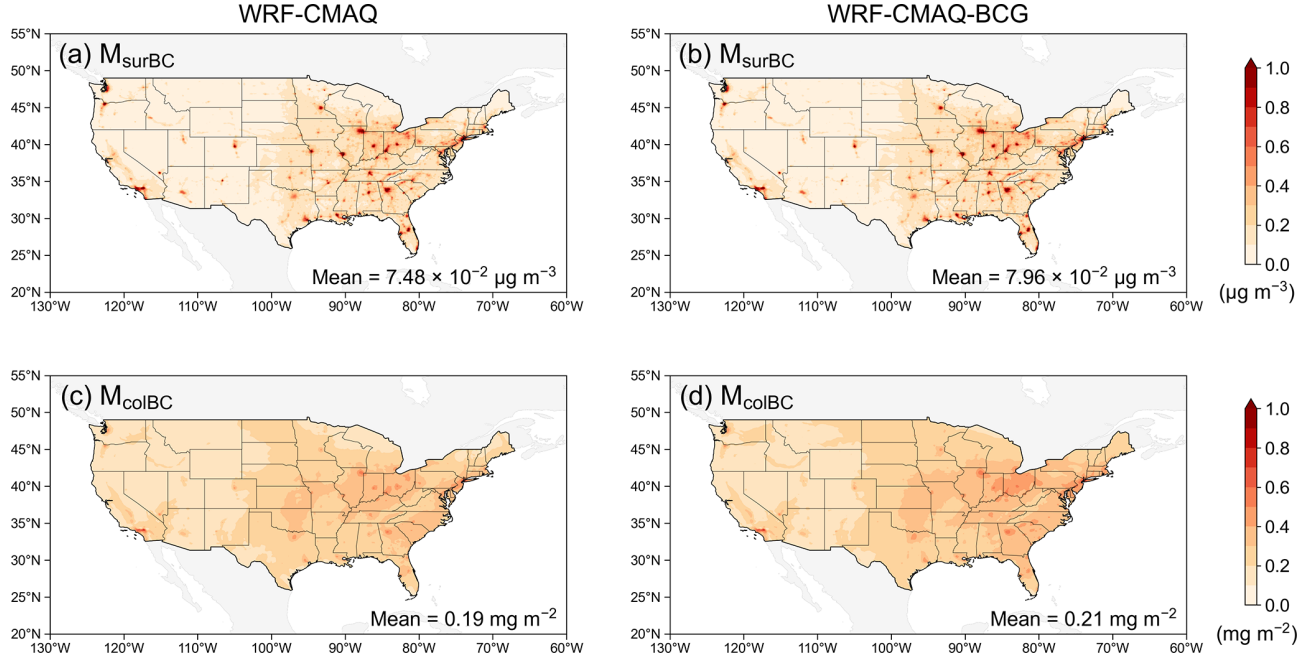

Figure 10. Spatial distribution of **(a, b)** surface BC mass concentration (M_{surBC}) and **(c, d)** column BC mass concentration (M_{colBC}) simulated by **(a, c)** the WRF-CMAQ model and **(b, d)** the WRF-CMAQ-BCG model, with average hourly values for June.

5 Conclusions

In this study, we developed the WRF-CMAQ-BCG model by integrating the BC aging process on top of the WRF-CMAQ model. This advancement involves the introduction of two distinct species, bare BC and coated BC, to characterize BC aging states and the development of a dedicated BC aging module. The aging process is represented by the conversion from bare BC to coated BC. Furthermore, we modified the wet-deposition module and aerosol optical module to investigate the effects of changes in hydrophobicity and light absorption properties described in the BC aging process.

Based on the WRF-CMAQ two-way coupled model, we conducted a simulation over the CONUS domain for June 2010 and performed regional and T0 site evaluations by undertaking comparison with multi-source observational data. The T0 site used for detailed analysis is located in Sacramento, California. The results indicate that the WRF-CMAQ-BCG model can provide reasonably accurate meteorological and chemical conditions for the BC aging process without compromising the computational accuracy of the original model. The results of our new module show the spatiotemporal variations in aging-related variables. The average aging rate is 2.26×10^{-5} s^{-1}, and the average aging

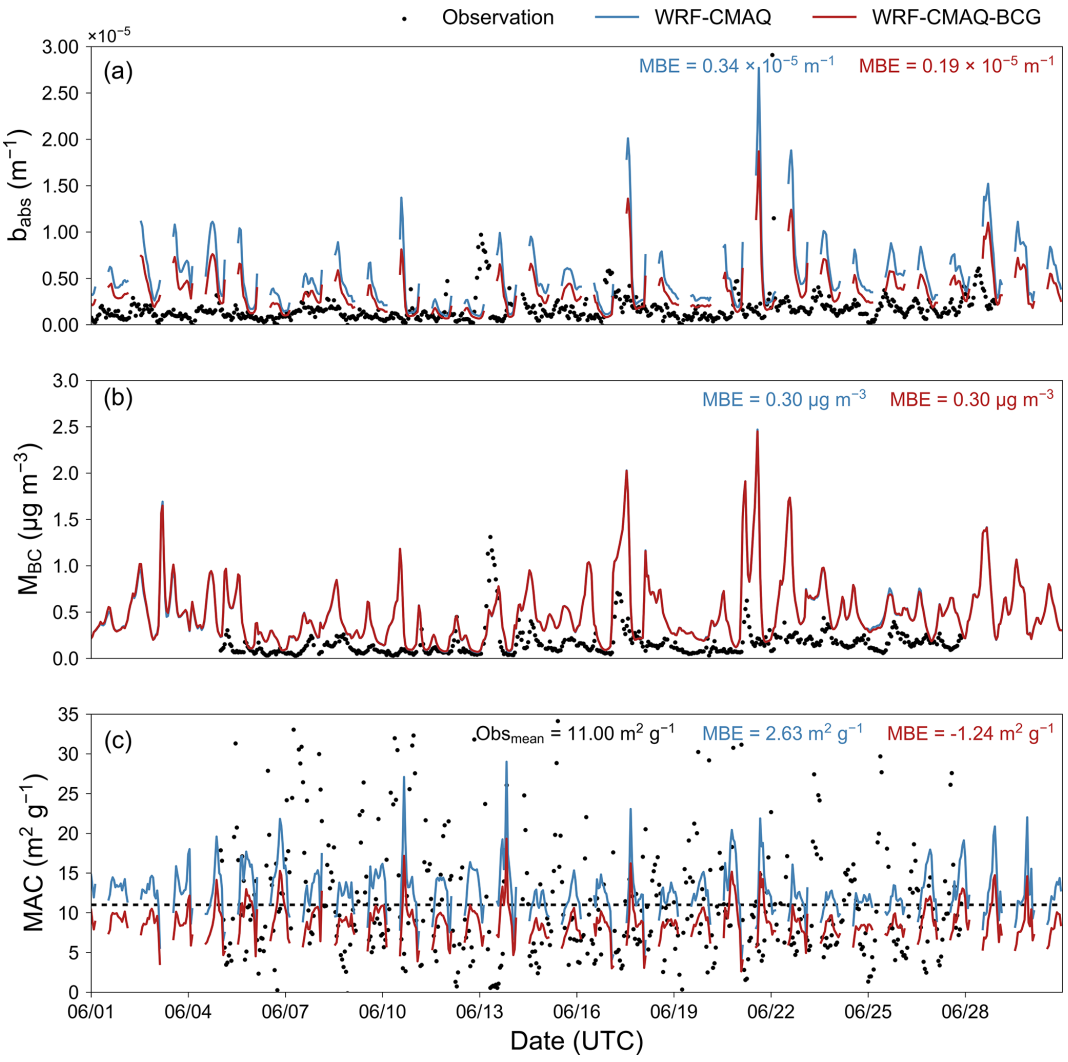

Figure 11. Time series comparison of the simulated and observed **(a)** absorption coefficient (b_{abs}), **(b)** BC mass concentration (M_{BC}), and **(c)** BC mass absorption cross-section (MAC).

timescale is 17.49 h. Furthermore, the aging process allows BC aerosol mixing states to exhibit certain temporal and spatial distribution characteristics. Spatial analysis of the WRF-CMAQ-BCG model outputs demonstrates a clear aging behavior: regions near emission sources exhibit a higher proportion of bare BC, whereas areas farther from these sources show a dominance of coated BC. The average number fraction of coated BC is approximately 57 %. For the temporal-variation characteristic, the number fraction of simulated coated BC shows a distinct increase during the daytime period.

BC aerosol undergoes a conversion in terms of its hydrophobic properties during the aging process, significantly impacting in-cloud scavenging mechanisms. Model simulations reveal distinct deposition patterns for different BC aging states: bare BC exhibits a localized, point-like wet-deposition pattern, while coated BC displays a more widespread zonal pattern. Notably, coated BC emerges as the primary contributor to overall BC aerosol wet deposition. In addition, the average BC wet deposition simulated by the WRF-CMAQ-BCG model in the US region is 3.02×10^{-2} mg m^{-2} d^{-1}, which is 17.7 % less than the 3.67×10^{-2} mg m^{-2} d^{-1} simulated by the WRF-CMAQ model. The reduction in BC wet deposition makes both the surface BC mass concentration and BC column concentration higher. The average BC column concentration of 0.19 mg m^{-2} in the WRF-CMAQ model increases to 0.21 mg m^{-2} in the WRF-CMAQ-BCG model, representing an increase of 10.5 %. This indicates that the fully internally mixed assumption in the WRF-CMAQ model, which does not account for the aging process, overestimates BC wet deposition and thus underestimates BC mass concentration.

The new model's ability to simulate the coexistence of externally mixed bare BC and internally mixed coated BC,

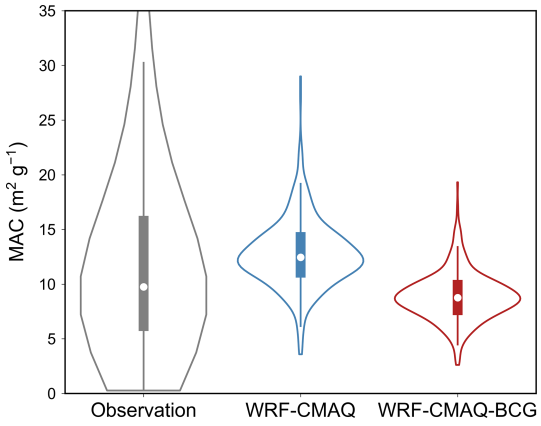

Figure 12. Statistical comparison of the simulated and observed BC mass absorption cross-section (MAC). The width of the violin plot reflects the distribution of the MAC values, while the rectangular shapes inside represent miniature box-and-whisker plots. The white dots denote the median values of the results for that category.

providing a better representation of atmospheric conditions, has prompted BC optical-property modification in the model. We compared the b_{abs} values calculated by both the WRF-CMAQ model and the WRF-CMAQ-BCG model with the observed values; their MBE values are 0.34×10^{-5} and $0.19 \times 10^{-5}\,m^{-1}$, respectively. Both the median and the mode MAC values derived from the new model showed better agreement with observations compared to the original model's outputs. In conclusion, the WRF-CMAQ-BCG model, which accounts for the BC aging process, enhances the capability to analyze aging-related variables and BC mixing state, as well as improves performance in terms of wet deposition and optical properties.

Code availability. The CMAQ model source codes are publicly available online at https://doi.org/10.5281/zenodo.7218076 (US EPA Office of Research and Development, 2022). The WRF-CMAQ-BCG model source codes and other codes for this study are available on Zenodo at https://doi.org/10.5281/zenodo.14187238 (Jin et al., 2024a).

Data availability. Our analytic data that provide the major results are available on Zenodo at https://doi.org/10.5281/zenodo.14192877 (Jin et al., 2024b).

Supplement. The supplement related to this article is available online at https://doi.org/10.5194/acp-25-2613-2025-supplement.

Author contributions. Conceptualization: JianW, CL; data curation: YJ, DCW, GS, KMF; formal analysis: JianW, JiapW, JC, CL; funding acquisition: JianW; investigation: JiapW, ZT, ShaW, ZZ; methodology: YJ, JianW, DCW, GS, KMF, CL; visualization: YJ; writing – original draft: YJ; writing – review and editing: YJ, JianW, DCW, CL, GS, KMF, ShaW, JiapW, JC, ZT, ZZ, JX, ShuW, AD.

Competing interests. The contact author has declared that none of the authors has any competing interests.

Disclaimer. The views expressed in this paper are those of the authors and do not necessarily reflect the views or policies of the US EPA.

Publisher's note: Copernicus Publications remains neutral with regard to jurisdictional claims made in the text, published maps, institutional affiliations, or any other geographical representation in this paper. While Copernicus Publications makes every effort to include appropriate place names, the final responsibility lies with the authors.

Acknowledgements. The model simulation was conducted in the High Performance Computing Center of the Nanjing University of Information Science & Technology. We acknowledge the observation data provided by the Carbonaceous Aerosol and Radiative Effects Study (CARES) campaign of the Atmospheric Radiation Measurement (ARM) program by the US Department of Energy (DOE), the Interagency Monitoring of Protected Visual Environments (IMPROVE) program, the Air Quality System (AQS) of the US Environmental Protection Agency (EPA), and the Polarization and Directionality of the Earth's Reflectances (POLDER) satellite mission by the French space agency (CNES).

Financial support. This research has been supported by the National Natural Science Foundation of China (grant nos. 42422505, 42475116, and 42075098), the National Key Research and Development Program of China (grant no. 2022YFC3701000, Task 5), and the Postgraduate Research and Practice Innovation Program of Jiangsu Province (grant no. KYCX23_1315).

Review statement. This paper was edited by Pablo Saide and reviewed by two anonymous referees.

References

Begam, G. R., Vachaspati, C. V., Ahammed, Y. N., Kumar, K. R., Babu, S. S., and Reddy, R. R.: Measurement and analysis of black carbon aerosols over a tropical semi-arid station in Kadapa, India, Atmos. Res., 171, 77–91, https://doi.org/10.1016/J.ATMOSRES.2015.12.014, 2016.

Bibi, S., Alam, K., Chishtie, F., Bibi, H., and Rahman, S.: Observations of black carbon aerosols characteristics over an urban environment: radiative forcing and related implications, Sci. Total Environ., 603–604, 319–329, https://doi.org/10.1016/J.SCITOTENV.2017.06.082, 2017.

Binkowski, F. S. and Roselle, S. J.: Models-3 Community Multiscale Air Quality (CMAQ) model aerosol component. 1. Model description, J. Geophys. Res., 108, 4183, https://doi.org/10.1016/J.SCITOTENV.2017.06.082, 2003.

Bond, T. C. and Bergstrom, R. W.: Light absorption by carbonaceous particles: An investigative review, Aerosol Sci. Tech., 40, 27–67, https://doi.org/10.1080/02786820500421521, 2006.

Bond, T. C., Doherty, S. J., Fahey, D. W., Forster, P. M., Berntsen, T., DeAngelo, B. J., Flanner, M. G., Ghan, S., Kärcher, B., Koch, D., Kinne, S., Kondo, Y., Quinn, P. K., Sarofim, M. C., Schultz, M. G., Schulz, M., Venkataraman, C., Zhang, H., Zhang, S., Bellouin, N., Guttikunda, S. K., Hopke, P. K., Jacobson, M. Z., Kaiser, J. W., Klimont, Z., Lohmann, U., Schwarz, J. P., Shindell, D., Storelvmo, T., Warren, S. G., and Zender, C. S.: Bounding the role of black carbon in the climate system: A scientific assessment, J. Geophys. Res.-Atmos., 118, 5380–5552, https://doi.org/10.1002/jgrd.50171, 2013.

Barrett, T. E., Ponette-González, A. G., Rindy, J. E., and Weathers, K. E.: Wet deposition of black carbon: A synthesis, Atmos. Environ., 213, 558–567, https://doi.org/10.1016/j.atmosenv.2019.06.033, 2019.

Cahill, J. F., Suski, K., Seinfeld, J. H., Zaveri, R. A., and Prather, K. A.: The mixing state of carbonaceous aerosol particles in northern and southern California measured during CARES and CalNex 2010, Atmos. Chem. Phys., 12, 10989–11002, https://doi.org/10.5194/acp-12-10989-2012, 2012.

Chen, G., Wang, J., Wang, Y., Wang, J., Jin, Y., Cheng, Y., Yin, Y., Liao H., Ding, A., Wang S., Hao J., and Liu, C.: An aerosol optical module with observation-constrained black carbon properties for global climate models, J. Adv. Model Earth Sy., 15, e2022MS003501, https://doi.org/10.1029/2022MS003501, 2023.

Choi, Y., Kanaya, Y., Takigawa, M., Zhu, C., Park, S.-M., Matsuki, A., Sadanaga, Y., Kim, S.-W., Pan, X., and Pisso, I.: Investigation of the wet removal rate of black carbon in East Asia: validation of a below- and in-cloud wet removal scheme in FLEXible PARTicle (FLEXPART) model v10.4, Atmos. Chem. Phys., 20, 13655–13670, https://doi.org/10.5194/acp-20-13655-2020, 2020.

Croft, B., Lohmann, U., and von Salzen, K.: Black carbon ageing in the Canadian Centre for Climate modelling and analysis atmospheric general circulation model, Atmos. Chem. Phys., 5, 1931–1949, https://doi.org/10.5194/acp-5-1931-2005, 2005.

Ding, A. J., Huang, X., Nie, W., Sun, J. N., Kerminen, V. M., Petäjä, T., Su, H., Cheng, Y. F., Yang, X.-Q., Wang, M. H., Chi, X. G., Wang, J. P., Virkkula, A., Guo, W. D., Yuan, J., Wang, S. Y., Zhang, R. J., Wu, Y. F., Song, Y., Zhu, T., Zilitinkevich, S., Kulmala, M., and Fu, C. B.: Enhanced haze pollution by black carbon in megacities in China, Geophys. Res. Lett., 43, 2873–2879, https://doi.org/10.1002/2016GL067745, 2016.

Doran, J. C., Fast, J. D., Barnard, J. C., Laskin, A., Desyaterik, Y., and Gilles, M. K.: Applications of lagrangian dispersion modeling to the analysis of changes in the specific absorption of elemental carbon, Atmos. Chem. Phys., 8, 1377–1389, https://doi.org/10.5194/acp-8-1377-2008, 2008.

Gilliam, R. C., Godowitch, J. M., and Rao, S. T.: Improving the horizontal transport in the lower troposphere with four dimensional data assimilation, Atmos. Environ., 53, 186–201, https://doi.org/10.1016/j.atmosenv.2011.10.064, 2012.

Hansen, J. and Nazarenko, L.: Soot climate forcing via snow and ice albedos, P. Natl. Acad. Sci. USA, 101, 423–428, https://doi.org/10.1073/pnas.2237157100, 2004.

He, C., Liou, K.-N., Takano, Y., Zhang, R., Levy Zamora, M., Yang, P., Li, Q., and Leung, L. R.: Variation of the radiative properties during black carbon aging: theoretical and experimental intercomparison, Atmos. Chem. Phys., 15, 11967–11980, https://doi.org/10.5194/acp-15-11967-2015, 2015.

He, C., Li, Q., Liou, K.-N., Qi, L., Tao, S., and Schwarz, J. P.: Microphysics-based black carbon aging in a global CTM: constraints from HIPPO observations and implications for global black carbon budget, Atmos. Chem. Phys., 16, 3077–3098, https://doi.org/10.5194/acp-16-3077-2016, 2016.

Huang, X.-F., Sun, T.-L., Zeng, L.-W., Yu, G.-H., and Luan, S.-J.: Black carbon aerosol characterization in a coastal city in South China using a single particle soot photometer, Atmos. Environ., 51, 21–28, https://doi.org/10.1016/j.atmosenv.2012.01.056, 2012a.

Huang, X.-F., He, L.-Y., Xue, L., Sun, T.-L., Zeng, L.-W., Gong, Z.-H., Hu, M., and Zhu, T.: Highly time-resolved chemical characterization of atmospheric fine particles during 2010 Shanghai World Expo, Atmos. Chem. Phys., 12, 4897–4907, https://doi.org/10.5194/acp-12-4897-2012, 2012b.

Huang, Y., Wu, S., Dubey, M. K., and French, N. H. F.: Impact of aging mechanism on model simulated carbonaceous aerosols, Atmos. Chem. Phys., 13, 6329–6343, https://doi.org/10.5194/acp-13-6329-2013, 2013.

Iacono, M. J., Delamere, J. S., Mlawer, E. J., Shephard, M. W., Clough, S. A., and Collins, W. D.: Radiative forcing by long-lived greenhouse gases: Calculations with the AER radiative transfer models, J. Geophys. Res.-Atmos., 113, D13103, https://doi.org/10.1029/2008JD009944, 2008.

Jacobson, M. Z.: Climate response of fossil fuel and biofuel soot, accounting for soot's feedback to snow and sea ice albedo and emissivity, J. Geophys. Res., 109, D21201, https://doi.org/10.1029/2004JD004945, 2004.

Jin, Y., Wang, J., Wong, D., Liu, C., Sarwar, G., Fahey, K., Wu, S., Wang, J., Cai, J., Tian, Z., Zhang, Z., Xing, J., Wang, S., and Ding, A.: The WRF-CMAQ-BCG model code, Zenodo [code], https://doi.org/10.5281/zenodo.14187238, 2024a.

Jin, Y., Wang, J., Liu, C., Wong, D., Sarwar, G., Fahey, K., Wu, S., Wang, J., Cai, J., Tian, Z., Zhang, Z., Xing, J., Wang, S., and Ding, A.: The WRF-CMAQ-BCG model data, Zenodo [data set], https://doi.org/10.5281/zenodo.14192877, 2024b.

Kain, J. S.: The Kain–Fritsch convective parameterization: an update, J. Appl. Meteorol., 43, 170–181, https://doi.org/10.1175/1520-0450(2004)043<0170:TKCPAU>2.0.CO;2, 2004.

Lack, D. A. and Cappa, C. D.: Impact of brown and clear carbon on light absorption enhancement, single scatter albedo and absorption wavelength dependence of black carbon, Atmos. Chem. Phys., 10, 4207–4220, https://doi.org/10.5194/acp-10-4207-2010, 2010.

Lan, Z. J., Huang, X. F., Yu, K. Y., Sun, T. L., Zeng, L. W., and Hu, M.: Light absorption of black carbon aerosol and its enhancement by mixing state in an urban atmosphere in South China, Atmos. Environ., 69, 118–123, https://doi.org/10.1016/j.atmosenv.2012.12.009, 2013.

Liu, J., Fan, S., Horowitz, L. W., and Levy, H.: Evaluation of factors controlling long-range transport of black carbon to the Arctic, J. Geophys. Res.-Atmos., 116, D04307, https://doi.org/10.1029/2010JD015145, 2011.

Liu, X., Easter, R. C., Ghan, S. J., Zaveri, R., Rasch, P., Shi, X., Lamarque, J.-F., Gettelman, A., Morrison, H., Vitt, F., Conley, A., Park, S., Neale, R., Hannay, C., Ekman, A. M. L., Hess, P., Mahowald, N., Collins, W., Iacono, M. J., Bretherton, C. S., Flanner, M. G., and Mitchell, D.: Toward a minimal representation of aerosols in climate models: description and evaluation in the Community Atmosphere Model CAM5, Geosci. Model Dev., 5, 709–739, https://doi.org/10.5194/gmd-5-709-2012, 2012.

Liu, X., Ma, P.-L., Wang, H., Tilmes, S., Singh, B., Easter, R. C., Ghan, S. J., and Rasch, P. J.: Description and evaluation of a new four-mode version of the Modal Aerosol Module (MAM4) within version 5.3 of the Community Atmosphere Model, Geosci. Model Dev., 9, 505–522, https://doi.org/10.5194/gmd-9-505-2016, 2016.

Monge, M. E., D'Anna, B., Mazri, L., Giroir-Fendler, A., Ammann, M., Donaldson, D. J., and George, C.: Light changes the atmospheric reactivity of soot, P. Natl. Acad. Sci. USA, 107, 6605–6609, https://doi.org/10.1073/pnas.0908341107, 2010.

Matsui, H., Koike, M., Kondo, Y., Moteki, N., Fast, J. D., and Zaveri, R. A.: Development and validation of a black carbon mixing state resolved three-dimensional model: Aging processes and radiative impact, J. Geophys. Res.-Atmos., 118, 2304–2326, https://doi.org/10.1029/2012JD018446, 2013.

Morrison, H., Thompson, G., and Tatarskii, V.: Impact of cloud microphysics on the development of trailing stratiform precipitation in a simulated squall line: Comparison of one-and two-moment schemes, Mon. Weather Rev., 137, 991–1007, https://doi.org/10.1175/2008MWR2556.1, 2009.

Oshima, N. and Koike, M.: Development of a parameterization of black carbon aging for use in general circulation models, Geosci. Model Dev., 6, 263–282, https://doi.org/10.5194/gmd-6-263-2013, 2013.

Oshima, N., Koike, M., Zhang, Y., Konda, Y., Moteki, N., Takegawa, N., and Miyazaki, Y.: Aging of black carbon in outflow from anthropogenic sources using a mixing state resolved model: Model development and evaluation, J. Geophys. Res.-Atmos., 114, D06210, https://doi.org/10.1029/2008JD010680, 2009.

Park, R. J., Jacob, D. J., Chin, M., and Martin, R. V.: Sources of carbonaceous aerosols over the United States and implications for natural visibility, J. Geophys. Res.-Atmos., 108, 4355, https://doi.org/10.1029/2002jd003190, 2003.

Peng, J., Hu, M., Guo, S., Du, Z., Zheng, J., Shang, D., Zamora, M. L., Zeng, L., Shao, M., Wu, Y. S., Zheng, J., Wang, Y., Glen, C. R., Collins, D. R., Molina, M. J., and Zhang, R.: Markedly enhanced absorption and direct radiative forcing of black carbon under polluted urban environments, P. Natl. Acad. Sci. USA, 113, 4266–4271, https://doi.org/10.1073/pnas.1602310113, 2016.

Pleim, J. E.: A simple, efficient solution of flux–profile relationships in the atmospheric surface layer, J. Appl. Meteorol. Clim., 45, 341–347, https://doi.org/10.1175/JAM2339.1, 2006.

Pleim, J. E.: A combined local and nonlocal closure model for the atmospheric boundary layer. Part I: Model description and testing, J. Appl. Meteorol. Clim., 46, 1383–1395, https://doi.org/10.1175/JAM2539.1, 2007.

Pleim, J. E. and Gilliam, R.: An indirect data assimilation scheme for deep soil temperature in the Pleim–Xiu land surface model, J. Appl. Meteorol. Clim., 48, 1362–1376, https://doi.org/10.1175/2009JAMC2053.1, 2009.

Pratt, K. A., Murphy, S. M., Subramanian, R., DeMott, P. J., Kok, G. L., Campos, T., Rogers, D. C., Prenni, A. J., Heymsfield, A. J., Seinfeld, J. H., and Prather, K. A.: Flight-based chemical characterization of biomass burning aerosols within two prescribed burn smoke plumes, Atmos. Chem. Phys., 11, 12549–12565, https://doi.org/10.5194/acp-11-12549-2011, 2011.

Ramanathan, V. and Carmichael, G.: Global and regional climate changes due to black carbon, Nat. Geosci., 1, 221–227, https://doi.org/10.1038/ngeo156, 2008.

Riemer, N., West, M., Zaveri, R. A., and Easter, R.: Simulating the evolution of soot mixing state with a particle-resolved aerosol model, J. Geophys. Res.-Atmos., 114, D09202, https://doi.org/10.1029/2008JD011073, 2009.

Riemer, N., West, M., Zaveri, R. A., and Easter, R.: Estimating black carbon aging time-scales with a particle-resolved aerosol model, J. Aerosol Sci., 41, 143–158, https://doi.org/10.1016/j.jaerosci.2009.08.009, 2010.

Shen, W., Wang, M., Liu, Y., Dong, X., Zhao, D., Yue, M., Tian, P., and Ding, D.: Evaluating BC Aging Processes in the Community Atmosphere Model Version 6 (CAM6), J. Geophys. Res.-Atmos., 128, e2022JD037427, https://doi.org/10.1029/2022JD037427, 2023.

Solmon, F., Giorgi, F., and Liousse, C.: Aerosol modelling for regional climate studies: application to anthropogenic particles and evaluation over a European/African domain, Tellus B, 58, 51–72, https://doi.org/10.1111/j.1600-0889.2005.00155.x, 2006.

Stevens, R. and Dastoor, A.: A review of the representation of aerosol mixing state in atmospheric models, Atmosphere, 1, 168, https://doi.org/10.3390/atmos10040168, 2019.

Tan, T., Guo, S., Wu, Z., He, L., Huang, X., and Hu M.: Impact of aging process on atmospheric black carbon aerosol properties and climate effects (in Chinese), Chin. Sci. Bull., 65, 4235–4250, https://doi.org/10.1360/TB-2020-0745, 2020.

Textor, C., Schulz, M., Guibert, S., Kinne, S., Balkanski, Y., Bauer, S., Berntsen, T., Berglen, T., Boucher, O., Chin, M., Dentener, F., Diehl, T., Easter, R., Feichter, H., Fillmore, D., Ghan, S., Ginoux, P., Gong, S., Grini, A., Hendricks, J., Horowitz, L., Huang, P., Isaksen, I., Iversen, I., Kloster, S., Koch, D., Kirkevåg, A., Kristjansson, J. E., Krol, M., Lauer, A., Lamarque, J. F., Liu, X., Montanaro, V., Myhre, G., Penner, J., Pitari, G., Reddy, S., Seland, Ø., Stier, P., Takemura, T., and Tie, X.: Analysis and quantification of the diversities of aerosol life cycles within AeroCom, Atmos. Chem. Phys., 6, 1777–1813, https://doi.org/10.5194/acp-6-1777-2006, 2006.

US EPA Office of Research and Development: CMAQ (5.4), Zenodo [code], https://doi.org/10.5281/zenodo.7218076, 2022.

Wang, Q., Huang, R. J., Cao, J., Han, Y., Wang, G., Li, G., Wang, Y., Dai, W., Zhang, R., and Zhou, Y.: Mixing state of black carbon aerosol in a heavily polluted urban area of China: implications for light absorption enhancement, Aerosol Sci. Tech., 48, 689–697, https://doi.org/10.1080/02786826.2014.917758, 2014a.

Wang, Q., Schwarz, J. P., Cao, J., Gao, R., Fahey, D. W., Hu, T., Huang, R.-J., Han Y., and Shen, Z.: Black carbon aerosol characterization in a remote area of Qinghai–Tibetan

Plateau, western China, Sci. Total Environ., 479, 151–158, https://doi.org/10.1016/j.scitotenv.2014.01.098, 2014b.

Wang, Q., Huang, R. J., Zhao, Z., Zhang, N., Wang, Y., Ni, H., Tie, X., Han, Y., Zhuang, M., Wang, M., Zhang, J., Zhang, X., Dusek, U., and Cao, J.: Size distribution and mixing state of refractory black carbon aerosol from a coastal city in South China, Atmos. Res., 181, 163–171, https://doi.org/10.1016/j.atmosres.2016.06.022, 2016.

Wang, Q., Cao, J., Han, Y., Tian, J., Zhu, C., Zhang, Y., Zhang, N., Shen, Z., Ni, H., Zhao, S., and Wu, J.: Sources and physicochemical characteristics of black carbon aerosol from the southeastern Tibetan Plateau: internal mixing enhances light absorption, Atmos. Chem. Phys., 18, 4639–4656, https://doi.org/10.5194/acp-18-4639-2018, 2018.

Wang, Y., Liu, F., He, C., Bi, L., Cheng, T., Wang, Z., Zhang, H., Zhang, X., Shi, Z., and Li, W.: Fractal dimensions and mixing structures of soot particles during atmospheric processing, Environ. Sci. Tech. Let., 4, 487–493, https://doi.org/10.1021/acs.estlett.7b00418, 2017.

Wang, Y., Li, W., Huang, J., Liu L., Pang, Y., He, C., Liu, F., Liu, D., Bi, L., Zhang, X., and Shi Z.: Nonlinear Enhancement of Radiative Absorption by Black Carbon in Response to Particle Mixing Structure, Geophys. Res. Lett., 48, e2021GL096437, https://doi.org/10.1029/2021GL096437, 2021.

Wong, D. C., Pleim, J., Mathur, R., Binkowski, F., Otte, T., Gilliam, R., Pouliot, G., Xiu, A., Young, J. O., and Kang, D.: WRF-CMAQ two-way coupled system with aerosol feedback: software development and preliminary results, Geosci. Model Dev., 5, 299–312, https://doi.org/10.5194/gmd-5-299-2012, 2012.

Yu, S.: Role of organic acids (formic, acetic, pyruvic and oxalic) in the formation of cloud condensation nuclei (CCN): a review, Atmos. Res., 53, 185–217, https://doi.org/10.1016/S0169-8095(00)00037-5, 2000.

Yuan, J., Modini, R. L., Zanatta, M., Herber, A. B., Müller, T., Wehner, B., Poulain, L., Tuch, T., Baltensperger, U., and Gysel-Beer, M.: Variability in the mass absorption cross section of black carbon (BC) aerosols is driven by BC internal mixing state at a central European background site (Melpitz, Germany) in winter, Atmos. Chem. Phys., 21, 635–655, https://doi.org/10.5194/acp-21-635-2021, 2021.

Zaveri, R. A., Barnard, J. C., Easter, R. C., Riemer, N., and West, M.: Particle-resolved simulation of aerosol size, composition, mixing state, and the associated optical and cloud condensation nuclei activation properties in an evolving urban plume, J. Geophys. Res.-Atmos., 115, D17210, https://doi.org/10.1029/2009JD013616, 2010.

Zaveri, R. A., Shaw, W. J., Cziczo, D. J., Schmid, B., Ferrare, R. A., Alexander, M. L., Alexandrov, M., Alvarez, R. J., Arnott, W. P., Atkinson, D. B., Baidar, S., Banta, R. M., Barnard, J. C., Beranek, J., Berg, L. K., Brechtel, F., Brewer, W. A., Cahill, J. F., Cairns, B., Cappa, C. D., Chand, D., China, S., Comstock, J. M., Dubey, M. K., Easter, R. C., Erickson, M. H., Fast, J. D., Floerchinger, C., Flowers, B. A., Fortner, E., Gaffney, J. S., Gilles, M. K., Gorkowski, K., Gustafson, W. I., Gyawali, M., Hair, J., Hardesty, R. M., Harworth, J. W., Herndon, S., Hiranuma, N., Hostetler, C., Hubbe, J. M., Jayne, J. T., Jeong, H., Jobson, B. T., Kassianov, E. I., Kleinman, L. I., Kluzek, C., Knighton, B., Kolesar, K. R., Kuang, C., Kubátová, A., Langford, A. O., Laskin, A., Laulainen, N., Marchbanks, R. D., Mazzoleni, C., Mei, F., Moffet, R. C., Nelson, D., Obland, M. D., Oetjen, H., Onasch, T. B., Ortega, I., Ottaviani, M., Pekour, M., Prather, K. A., Radney, J. G., Rogers, R. R., Sandberg, S. P., Sedlacek, A., Senff, C. J., Senum, G., Setyan, A., Shilling, J. E., Shrivastava, M., Song, C., Springston, S. R., Subramanian, R., Suski, K., Tomlinson, J., Volkamer, R., Wallace, H. W., Wang, J., Weickmann, A. M., Worsnop, D. R., Yu, X.-Y., Zelenyuk, A., and Zhang, Q.: Overview of the 2010 Carbonaceous Aerosols and Radiative Effects Study (CARES), Atmos. Chem. Phys., 12, 7647–7687, https://doi.org/10.5194/acp-12-7647-2012, 2012.

Zhang, F., Wang, Y., Peng, J., Chen, L., Sun, Y., Duan, L., Ge, X., Li, Y., Zhao, J., Liu, C., Zhang, A. L., Ji, Y., Wang, G., Hu, M., Molina, M. J., and Zhang, R.: An unexpected catalyst dominates formation and radiative forcing of regional haze, P. Natl. Acad. Sci. USA, 117, 3960–3966, https://doi.org/10.1073/pnas.1919343117, 2020.

Zhang, Y., Su, H., Ma, N., Li, G., Kecorius, S., Wang, Z., Hu, M., Zhu, T., He, K., Wiedensohler, A., Zhang, Q., and Cheng, Y.: Sizing of ambient particles from a single-particle soot photometer measurement to retrieve mixing state of black carbon at a regional site of the North China plain, J. Geophys. Res.-Atmos., 123, 12–778, https://doi.org/10.1029/2018JD028810, 2018.